Analytical solution for mode-mismatched thermal lens spectroscopy with sample-fluid heat coupling

Luis C. Malacarne,[1,a)] Nelson G. C. Astrath,[1,b)] Paulo R. B. Pedreira,[1] Renio S. Mendes,[1] Mauro L. Baesso,[1] Prakash R. Joshi,[2] and Stephen E. Bialkowski[2]
[1]*Departamento de Física, Universidade Estadual de Maringá, Maringá-PR 87020-900, Brazil*
[2]*Department of Chemistry and Biochemistry, Utah State University, Logan, Utah 84322-0300, USA*

(Received 30 September 2009; accepted 11 January 2010; published online 3 March 2010)

This paper presents an improved theoretical description of the mode-mismatched thermal lens effect using models that account for heat transport both within the sample and out to the surrounding coupling medium. Analytical and numerical finite element analysis (FEA) solutions are compared and subsequently used to model the thermal lens effect that would be observed using continuous laser excitation. FEA model results were found to be in excellent agreement with the analytical solutions. The model results show that heat transfer to the air coupling medium introduces only a minor effect when compared with the solution obtained without considering axial air-sample heat flux for practical examples. On the other hand, the thermal lens created in the air coupling fluid has a relatively more significant effect on the time-dependent photothermal lens signals.
 [doi:10.1063/1.3309762]

I. INTRODUCTION

Thermal lens (TL) spectroscopy is a remote, nondestructive, fast, and highly sensitive photothermal technique[1–13] for the measurement of optical absorption and thermo-optical properties of materials. This technique has been applied to obtain optical and thermal-optical properties of a wide range of material, including glasses, oils, polymers, and liquid crystals.[7–13] TL technique has also been demonstrated as a powerful method for chemical analysis.[4,8]

Theoretical analytical solutions restricted the use of TL spectroscopy to low optical absorbing samples. Recently, a simple approximation was proposed by taking the high optical absorbing material case into account[14] and also the complementary thermal mirror method[15–18] was developed to be used concurrently with TL leading to additional information about physical properties of high and low absorbing samples. Despite numerous applications and theoretical descriptions, TL model has no analytical solution that considers the axial heat coupling between sample and external medium into account. Recently,[19–21] by using finite element analysis (FEA), it has been demonstrated that the effect of surface heat transfer from sample to the surroundings could introduce some modification in the physical parameters measured by pulsed laser excited photothermal lens spectroscopy.

In this work, we present a semianalytical theoretical description of the mode-mismatched TL effect by taking the coupling of heat both within the sample and out to the surroundings into account. Our analytical results are compared with FEA solutions. These two methods for calculating the time- and space-dependent heat transfer are in excellent agreement lending some degree of confidence in the predictions of these solutions. We show that the interface effect occurs in finite characteristic lengths. For samples with thickness larger than this characteristic length, a simplified solution can be used to obtain the TL phase shift within the sample and surrounding fluid.

[a)]Electronic mail: lcmala@dfi.uem.br.
[b)]Electronic mail: astrathngc@pq.cnpq.br.

II. THEORY

A typical configuration used in mode-mismatched TL spectrometry is illustrated in Fig. 1(a). A continuous Gaussian excitation laser beam irradiates a weakly absorbing sample of thickness l, causing a TL. A second, often weaker Gaussian beam propagates through the sample collinear to the excitation laser and is affected by the TL. The characteristic electric field radii of the excitation and probe beams in the sample are ω_{0e} and ω_{1P}, respectively. The probe beam propagates in the $+z$-direction, and the sample is centered at $z=0$. The distance between the sample and the detector plane is Z_2 and the distance between the sample and the minimum probe beam waist of a radius ω_{0P} is Z_1. In this configuration, it is assumed that (i) the sample dimensions are large compared to the excitation beam radius to avoid edge effects; (ii) the absorbed excitation laser energy by the sample is low so that the excitation laser can be considered to be uniform along the z-direction.

A. Temperature gradient

To model the sample-fluid heating coupling, let us consider two semi-infinity spaces with boundaries at $z=0$ with the sample in the $0<z<\infty$ region and the fluid (air in this work) in the $-\infty<z<0$ region. The temperature rise distributions inside the sample, $T_s(r,z,t)$, and in the fluid, $T_f(r,z,t)$, are given by the solution of the heat conduction differential equations,

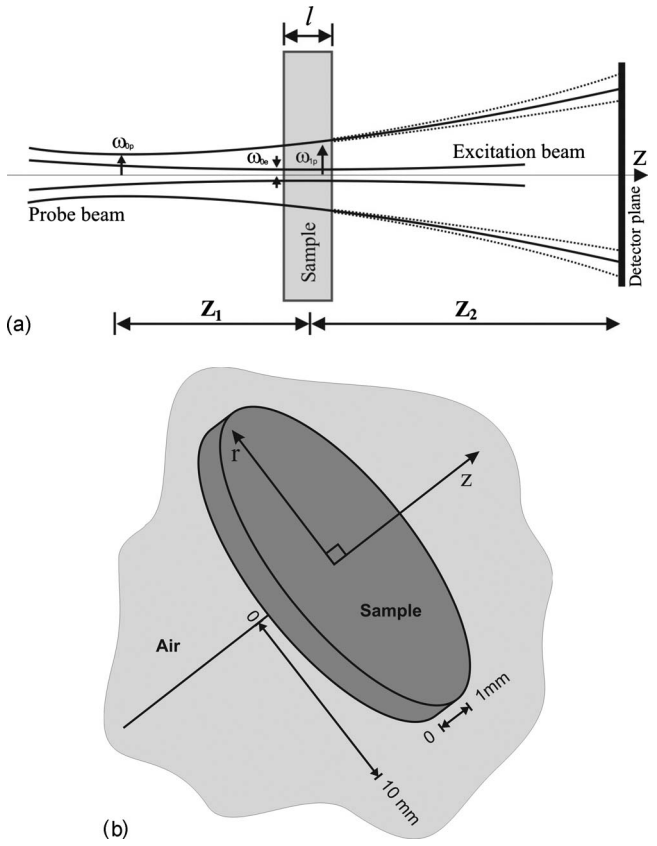

FIG. 1. (a) Scheme of the geometric positions of the beams in a mode-mismatched dual-beam TL experiment and (b) sample geometry used for the FEA modeling.

$$\frac{\partial T_s(r,z,t)}{\partial t} - D\nabla^2 T_s(r,z,t) = Q(r,z), \tag{1}$$

$$\frac{\partial T_f(r,z,t)}{\partial t} - D_f\nabla^2 T_f(r,z,t) = 0. \tag{2}$$

The boundary and initial conditions are given by

$$k\partial_z T_s(r,z,t)|_{z=0} = k_f\partial_z T_f(r,z,t)|_{z=0}$$

$$T_s(\infty,z,t) = T_s(r,\infty,t) = 0,$$

$$T_s(r,z,0) = T_f(r,z,0) = 0,$$

$$T_s(r,0,t) = T_f(r,0,t),$$

$$T_f(\infty,z,t) = T_f(r,-\infty,t) = 0. \tag{3}$$

$D_i = k_i/\rho_i c_i$ is the thermal diffusivity of the material i (sample and fluid). c_i, ρ_i, and k_i are the specific heat, mass density, and thermal conductivity of the material i, respectively. The Gaussian excitation laser profile is $Q(r,z) = Q_0 Q(r) Q(z)$, where $Q(r) = \exp(-2r^2/\omega^2)$, $Q_0 = 2P_e A_e \phi/\pi c\rho\omega^2$, P_e is the excitation beam power, A_e is the exponential optical absorption coefficient at excitation beam wavelength λ_e, $\phi = 1 - \eta\lambda_e/\langle\lambda_{em}\rangle$, where $\langle\lambda_{em}\rangle$ is the average wavelength of the fluorescence emission, and η is the fluorescence quantum efficiency, which competes for a share of absorbed excitation energy. $Q(z) = \exp(-A_e z)$ is the sample absorptance. For the purposes here, the optical absorption coefficient is small and $Q(z) = 1$ can be assumed.

Using Laplace and Hankel integral transform methods with the boundary conditions in Eq. (3), the solution of the heat conduction differential equations in the Laplace–Hankel space can be written as

$$T_s(\alpha,z,s) = -\frac{Q(\alpha)(k_f\sqrt{D}/k\sqrt{D_f})\sqrt{s+D_f\alpha^2}}{s(s+D\alpha^2)\left(1+\dfrac{k_f\sqrt{D}\sqrt{s+D_f\alpha^2}}{k\sqrt{D_f}\sqrt{s+D\alpha^2}}\right)} \times \frac{e^{-z\sqrt{(s+D\alpha^2)/D}}}{\sqrt{s+D\alpha^2}} + \frac{Q(\alpha)}{s(s+D\alpha^2)}, \tag{4}$$

and

$$T_f(\alpha,z,s) = -\frac{Q(\alpha)\sqrt{s+D_f\alpha^2}}{s(s+D\alpha^2)\left(1+\dfrac{k_f\sqrt{D}\sqrt{s+D_f\alpha^2}}{k\sqrt{D_f}\sqrt{s+D\alpha^2}}\right)} \times \frac{e^{-z\sqrt{(s+D_f\alpha^2)/D_f}}}{\sqrt{s+D_f\alpha^2}}. \tag{5}$$

Here, $Q(\alpha) = Q_0 \exp(-\omega^2\alpha^2/8)\omega^2/4$ comes from the Hankel transform of the source term. If $k_f\sqrt{D}\sqrt{s+D_f\alpha^2} \ll k\sqrt{D_f}\sqrt{s+D\alpha^2}$, the term in the denominator of Eqs. (4) and (5) can be expanded in series as $(1+x)^{-1} = 1 - x + x^2 + O(x^3)$. This assumption is fulfilled in the case of glass-air system. Thus, Eq. (4) can be written as

$$T_s(\alpha,z,s) = -Q(\alpha)\frac{k_f\sqrt{D}}{k\sqrt{D_f}}\frac{\sqrt{s+D_f\alpha^2}}{s(s+D\alpha^2)}\left(1 - \frac{k_f\sqrt{D}\sqrt{s+D_f\alpha^2}}{k\sqrt{D_f}\sqrt{s+D\alpha^2}} + \cdots\right)\frac{e^{-z\sqrt{(s+D\alpha^2)/D}}}{\sqrt{s+D\alpha^2}} + \frac{Q(\alpha)}{s(s+D\alpha^2)}, \tag{6}$$

and Eq. (5) becomes

$$T_f(\alpha,z,s) = -Q(\alpha)\frac{\sqrt{s+D_f\alpha^2}}{s(s+D\alpha^2)}\left(1 - \frac{k_f\sqrt{D}\sqrt{s+D_f\alpha^2}}{k\sqrt{D_f}\sqrt{s+D\alpha^2}} + \cdots\right)\frac{e^{-z\sqrt{(s+D_f\alpha^2)/D_f}}}{\sqrt{s+D_f\alpha^2}}. \tag{7}$$

The time-dependent temperatures are given by the inverse Laplace and Hankel transforms of Eqs. (6) and (7). Taking the expansion in Eqs. (6) and (7) up to the first, the temperature gradient within the sample, $T_{1(s)}(r,z,t)$, is given by the integral equation

$$T_{1(s)}(r,z,t) = Q_0 \int_0^t \int_0^\infty \frac{e^{-\omega^2\alpha^2/8}\omega^2}{4} \alpha J_0(\alpha r) \left[e^{-D\tau\alpha^2} - \frac{k_f\sqrt{D}}{k\sqrt{D_f}} e^{-D(t-\tau)\alpha^2} \frac{e^{-z^2/4D(t-\tau)}}{\sqrt{\pi(t-\tau)}} \left(\frac{\sqrt{D_f}\,\mathrm{erf}(\sqrt{\tau}\alpha\sqrt{D_f - D}) - e^{-D\tau\alpha^2}\sqrt{D_f - D}\,\mathrm{erf}(\sqrt{\tau}\alpha\sqrt{D_f - D})}{\alpha D} \right) \right] d\alpha d\tau, \tag{8}$$

while that for the coupling fluid, $T_{1(f)}(r,z,t)$, is

$$T_{1(f)}(r,z,t) = Q_0 \int_0^t \int_0^\infty \frac{e^{-\omega^2\alpha^2/8}\omega^2}{4} e^{-D_f(t-\tau)\alpha^2} \frac{e^{-z^2/4D_f(t-\tau)}}{\sqrt{\pi(t-\tau)}} \left[\frac{\sqrt{D_f}\,\mathrm{erf}(\sqrt{\tau}\alpha\sqrt{D_f}) - e^{-D\tau\alpha^2}\sqrt{D_f - D}\,\mathrm{erf}(\sqrt{\tau}\alpha\sqrt{D_f - D})}{\alpha D} - \frac{k_f\sqrt{D}}{k\sqrt{D_f}} \left(\frac{2e^{-D\tau\alpha^2}\sqrt{\tau}(D - D_F)}{D\sqrt{\pi}} + \frac{\mathrm{erf}(\sqrt{\tau}\alpha\sqrt{D})D_f}{D^{3/2}\alpha} \right) \right] \alpha J_0(\alpha r) d\alpha d\tau. \tag{9}$$

$J_n(x)$ is the Bessel function of the first kind and $\mathrm{erf}(x)$ is the error function.

Considering the zero-order expansion, which corresponds to the case where there is no heat flux from sample to air, i.e., $\partial_z T(r,z,t)|_{z=0}=0$, Eq. (8) becomes

$$T_{0(s)}(r,t) = \int_0^t \left(\frac{Q_0}{(1+2\tau/t_c)} \right) \exp\left(-\frac{2r^2/\omega_{0e}^2}{1+2\tau/t_c} \right) d\tau. \tag{10}$$

Equation (10) is the temperature solution commonly used to describe TL and thermal mirror effects for low absorbing semitransparent solids.[9,15–17] In addition, the zero-order approximation for the air temperature solution, which corresponds to the solution for a semispace system with the temperature in $z=0$ surface fixed by the sample's temperature, is given by

$$T_{0(f)}(r,z,t) = Q_0 \int_0^t \int_0^\infty \frac{e^{-\omega^2\alpha^2/8}\omega^2}{4e^{D_f(t-\tau)\alpha^2}} \frac{e^{-z^2/4D_f(t-\tau)}}{\sqrt{\pi(t-\tau)}} \left[\frac{\sqrt{D_f}\,\mathrm{erf}(\sqrt{\tau}\alpha\sqrt{D_f}) - e^{-D\tau\alpha^2}\sqrt{D_f - D}\,\mathrm{erf}(\sqrt{\tau}\alpha\sqrt{D_f - D})}{\alpha D} \right] \alpha J_0(\alpha r) d\alpha d\tau. \tag{11}$$

B. Finite element analysis

In order to ascertain the accuracy of our approximation, the space and time dependences of the temperature equations for air and sample in Eqs. (8) to (11) are compared with the FEA modeling solutions for a system with glass sample of thickness l surrounded by air. FEA software provides numerical solutions to the heat transfer equations with the realistic boundary conditions imposed by the experimental geometry. To better understand the transient temperature profile in the samples, FEA is used to model temperature changes. Results from the FEA calculations are then compared with the semi-infinity (Sec. II A) analytical solutions to gauge the error. COMSOL MULTIPHYSICS 3.5 analysis is carried out on a Dell Studio XPS 435, i7 940 processor, using MS WINDOWS VISTA. The numerical integrations in Eqs. (8)–(11) are performed using the standard functions in MATHEMATICA (version 7.0) software.

The COMSOL MULTIPHYSICS software in conduction and convection mode solves the heat diffusion equation given as

$$\rho c \frac{\partial T(r,z,t)}{\partial t} - k\nabla^2 T(r,z,t) = \rho c Q(r,z) - \cancel{\rho c u \cdot \nabla T(r,z,t)}, \tag{12}$$

in which u is the flow velocity. All other symbols are the same as those introduced above. Note that Eqs. (1), (2), and (12) differ only by the second term on the right side of the equation. This term can account for convection or mass flow heat transfer, which is not important for glasses.

FEA modeling consists of drawing the sample geometry and specifying material boundary conditions, heat sources, and sinks. The problems are then solved with rough finite element definition and further refinement of elements and domain are made. The element mesh is refined until model results become independent of mesh size. Finally, $T(r,z,t)$ can be obtained either at a single time, over a time series, or at steady state. The model solid absorbing media was cylindrical plate of 10 mm in diameter and 1 mm thick. Optical excitation was along the z-axis. The values of the thermal, optical, and mechanical parameters used for the analytical and FEA modeling simulations are shown in Table I.

Figure 2 shows the radial temperature profile within the glass sample at its center at $z=0.5$ mm. The results by the FEA model are compared with the temperature solution considering heat flux from glass to air, Eq. (8), at different exposure times. There is apparently little difference between the temperatures produced from the FEA model and the semi-infinite approximation with glass-air heat coupling.

Figure 3 shows the temperature profiles along the z-direction (air-glass-air) using the FEA modeling, the solution considering air surroundings, Eq. (8), and the solution with no transfer of heat from glass to air, Eq. (10), at different exposure times at $r=0$. It clearly shows an excellent agreement between the analytical solutions considering air coupling [Eqs. (8) and (9)] and the FEA model. On the other hand, as expected, there is a little difference for the predictions considering no heat transfer from glass to air, Eq. (10).

TABLE I. Parameters used for the simulations. The thermal, optical, and mechanical properties listed below are associated to characteristics values found in glasses (Refs. 12 and 18) and for the surrounding medium we use the air properties (Ref. 22).

P_e	(mW)	161
A_e	(m^{-1})	93
D	(10^{-7} m^2/s)	5
k	(W/mK)	1.4
ρ	(kg/m^3)	933
c	(J/kg K)	3000
D_f	(10^{-5} m^2/s)	2.2
k_f	(W/mK)	0.026
ds/dT	(10^{-6} K^{-1})	10
m		60
ρ_f	(kg/m^3)	1.18
c_f	(J/kg K)	1005
ω	(μm)	50
$t_c=\omega^2/4D$	(ms)	1.25
ϕ		0.6
α_T	(10^{-6} K^{-1})	7.5
ν		0.25
Q_0	(W K s^{-1})	818.803 56
$(dn/dT)_f$	(10^{-6} K^{-1})	−1
V		5

This difference is more evident close to the boundary sample-air. In the case of glass-air interface, the characteristic length is around $z=0.2$ mm into the sample. Deeper than that the temperature is the same as that one with no axial heat flux as long as the excitation beam waist is small relative to sample thickness. This shows that the interfaces do not affect each other if the sample is thick relative to the beam waist. Subsequently, the single-surface approximation used for the analytical model is valid for these conditions.

The same behavior is also observed for different radial positions, as shown in Fig. 4 at $t=0.12$ s. It is interesting to note the excellent agreement between FEA modeling and the analytical solution, Eqs. (8) and (9).

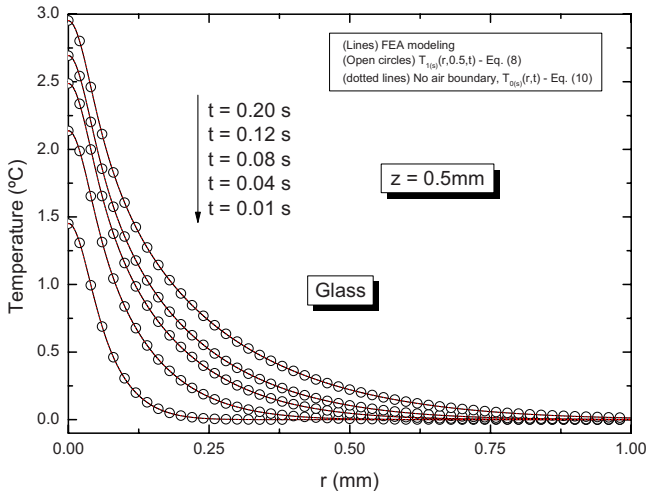

FIG. 2. (Color online) Temperature profile in the glass sample at $z=0.5$ mm using the FEA modeling, the solution considering heat flux to air, Eq. (8), and the solution with no transfer of heat from glass to air, Eq. (10), at different exposure times.

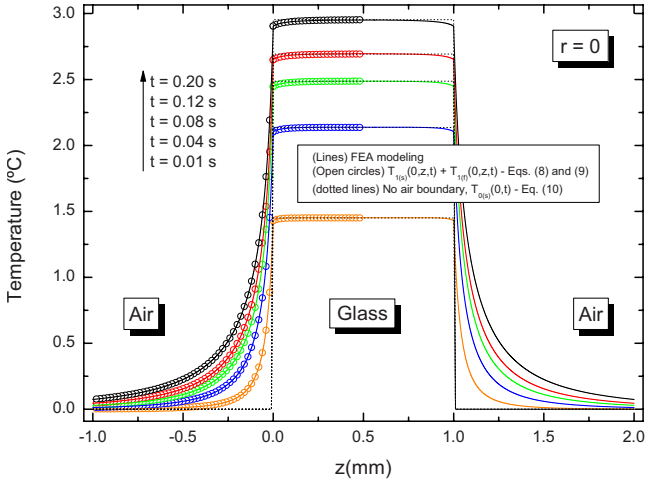

FIG. 3. (Color online) Temperature profile along the z direction (air-glass-air) using the FEA modeling, the solution considering air surroundings, Eqs. (8) and (9), and the solution with no transfer of heat from glass to air, Eq. (10), at different exposure times. $r=0$ was used in the simulations.

Figure 5 displays the radial temperature profile in the air using the FEA modeling and the solution for air, Eq. (9), at the sample surface in the air side from $z=0$ to 200 μm. The exposure time was $t=0.12$ s. Again, agreement between both the FEA and analytical modeling predictions, is good.

The results obtained using the FEA model show that the first order analytical approximation presented in this work can be used to describe the temperature profile in the sample and in the air surrounding it, at least in cases where binomial expansion is valid. In addition, the order zero approximation also represents quite well the temperature in the sample for thick samples. The density plot illustrated in Fig. 6 shows the complete solution for both the FEA and analytical approximation models within both air and sample.

III. PROBE BEAM PHASE SHIFT AND TL INTENSITY

The temporal and radial distribution of the temperature rise inside the sample and in the air induce a refractive index

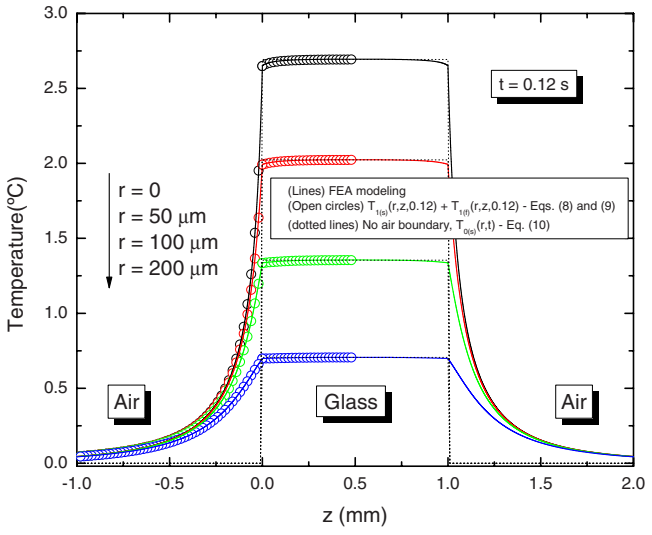

FIG. 4. (Color online) Temperature profile along the z direction (air-glass-air) using the FEA modeling, the solution considering air surroundings, Eqs. (8) and (9), and the solution with no transfer of heat from glass to air, Eq. (10), for different radial positions.

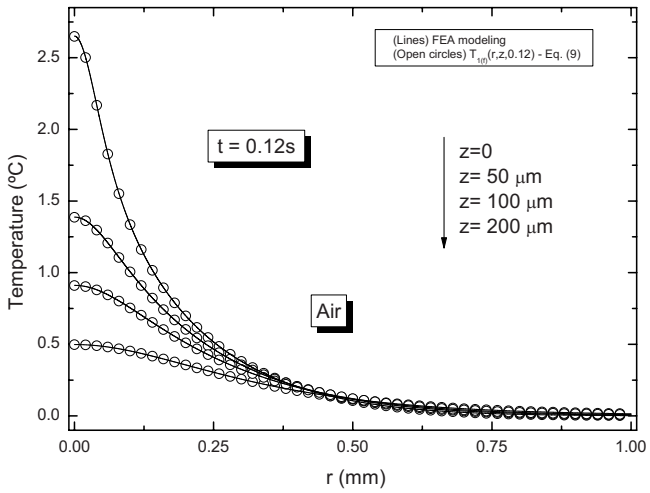

FIG. 5. (Color online) Radial temperature profile in the air surroundings at $t=0.12$ s using the FEA modeling, the solution for the air fluid, Eq. (9), at the sample surface in the air side, $z=0$, and up to 200 μm distant from there.

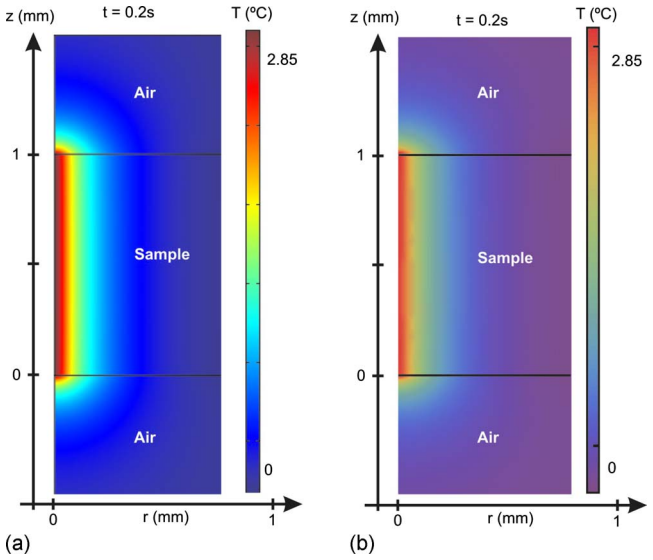

FIG. 6. (Color online) Density plot using (a) the FEA and (b) the analytical approximation models.

gradient, acting as an optical element, causing a phase shift Φ to the probe beam. The solutions presented in Eqs. (8) and (9) can be analytically used to describe theoretically the TL effect, by calculating the phase shift of the probe beam after passing thought the TL region and, therefore, to express the TL intensity signal.

For low optical absorbing samples, we can use our semi-infinite solution for the temperature, given by Eq. (8), to obtain the phase shift for finite sample of thickness l by the following equations:

$$\Phi_{(s)}(r,t) = \frac{2\pi}{\lambda_P}\frac{ds}{dT} 2\int_0^{l/2} [T(r,z,t) - T(0,z,t)]dz, \tag{13}$$

where the integration is from $0<z<l/2$, however multiplied by a factor of 2. ds/dT is the temperature coefficient of the optical path length at the probe beam wavelength λ_p. For the air domain

$$\Phi_{(f)}(r,t) = \frac{2\pi}{\lambda_P}\left(\frac{dn}{dT}\right)_f 2\int_{-\infty}^{0} [T_f(r,z,t) - T_f(0,z,t)]dz. \tag{14}$$

Here the factor of 2 accounts for the layers of air on both sides of the sample and $(dn/dT)_f$ is the temperature coefficient of the refractive index of the air. The total phases shift, $\Phi(r,t)=\Phi_{(s)}(r,t)+\Phi_{(f)}(r,t)$, describes the distortion of the probe beam caused by the temperature change in the medium.

Substituting Eq. (8) into Eq. (13) and performing the z integration, one gets the first order phase shift in the sample as

$$\Phi_{1(s)}(g,t) = \theta_s \int_0^{\infty} \frac{-e^{-\omega^2\alpha^2/8}\omega^2}{4}\frac{\sqrt{D}}{\alpha D}\frac{k_f\sqrt{D}}{k\sqrt{D_f}}\int_0^t \left\{ [e^{-D(t-\tau)\alpha^2}\mathrm{erf}[l/(4\sqrt{D}\sqrt{t-\tau})](\sqrt{D_f}\,\mathrm{erf}(\sqrt{\tau}\alpha\sqrt{D_f}) \right.$$
$$\left. - e^{-D\tau\alpha^2}\sqrt{D_f - D}\,\mathrm{erf}(\sqrt{\tau}\alpha\sqrt{D_f - D}))]d\tau + \frac{e^{-\omega^2\alpha^2/8}\omega^2}{4}\frac{l}{2}e^{-D\tau\alpha^2} \right\} \alpha[\mathrm{J}_0(\alpha\omega\sqrt{mg}) - 1]d\alpha. \tag{15}$$

Alternatively, Eq. (9) into Eq. (14), and performing the z and the time integrations, one gets the first order phase shift in the air as

$$\Phi_{1(f)}(g,t) = \theta_f \int_0^{\infty} \frac{e^{-\omega^2\alpha^2/8}\omega^2}{4}\left[\frac{\sqrt{D_f}}{\alpha D}\left(\frac{\mathrm{erf}(\sqrt{t}\alpha\sqrt{D_f})}{\alpha^2\sqrt{D_f}} - \frac{e^{-Dt\alpha^2}\sqrt{t}\,\mathrm{erfi}(\sqrt{t}\alpha\sqrt{D - D_f})}{\alpha^2 D\sqrt{D - D_f}} \right) \right.$$
$$\left. - \sqrt{D_f}\frac{k_f\sqrt{D}}{k\sqrt{D_f}}\left(\frac{-2\alpha\sqrt{D/\pi}e^{-Dt\alpha^2}\sqrt{t} + \mathrm{erf}(\sqrt{t}\alpha\sqrt{D})}{D^{3/2}\alpha^3} \right) \right] \alpha[\mathrm{J}_0(\alpha\omega\sqrt{mg}) - 1]d\alpha. \tag{16}$$

erfi(x) is the imaginary error function, $g=(r/\omega_{1P})^2$, $m=\omega_{1P}^2/\omega^2$ indicates the degree of the mode mismatching of probe and excitation beams, $\theta_f=(4\pi/\lambda_p)(dn/dT)_f Q_0$ and $\theta_s=(4\pi/\lambda_p)(ds/dT)Q_0$. Using Eqs. (10) and (11) one can write the zero-order approximation for the phase shift in the air and sample as

$$\Phi_{0(s)}(g,t)=\theta_s\frac{l\omega^2}{16D}\left[Ei(-2mg)-Ei\left(-\frac{2mg\omega^2}{\omega^2+8Dt}\right)+\log(\omega^2)-\log(\omega^2+8Dt)\right], \tag{17}$$

in which $Ei(x)$ is the exponential integral function, and

$$\Phi_{0(f)}(g,t)=\theta_f\int_0^\infty\frac{e^{-\omega^2\alpha^2/8}\omega^2}{4}\left[\frac{\sqrt{D_f}}{\alpha D}\left(\frac{\mathrm{erf}(\sqrt{t}\alpha\sqrt{D_f})}{\alpha^2\sqrt{D_f}}-\frac{e^{-Dt\alpha^2}\sqrt{t}\,\mathrm{erfi}(\sqrt{t}\alpha\sqrt{D-D_f})}{\alpha^2 D\sqrt{D-D_f}}\right)\right]\times\alpha[\mathrm{J}_0(\alpha\omega\sqrt{mg})-1]d\alpha. \tag{18}$$

Equation (17) is the phase shift commonly used to describe the TL effect[7] for low optical absorbing solids.

The complex electric field of a TEM_{00} Gaussian probe beam emerging from the sample can be expressed as[3]

$$U_P(r,Z_1)=B\exp\left[-i\left(\frac{\pi}{\lambda_P}\frac{r^2}{R_{1P}}+\Phi\right)-\frac{r^2}{\omega_{1P}^2}\right], \tag{19}$$

with $B=\omega_{1P}^{-1}\sqrt{2P_P/\pi}\exp(-i2\pi Z_1/\lambda_P)$. P_P and R_{1P} are the probe beam power and the radius of curvature of the probe beam at Z_1. The propagation of the emerged probe beam from the sample to the detector plane can be treated as a diffraction phenomenon. Using Fresnel diffraction theory, its complex amplitude at the detector plane can be obtained as described in Ref. 3. In this work only the center point of the probe beam at the detector plane is considered. Then, the complex amplitude of the probe beam at the center, using cylindrical coordinates, is given by 3,

$$U(Z_1+Z_2,t)=C\int_0^\infty\exp[-(1+iV)g-i\Phi_{(s)}(g,t)-i\Phi_{(f)}\times(g,t)]dg, \tag{20}$$

when $Z_2\ll Z_c$. Here, $V=Z_1/Z_C$ and Z_C is the confocal distance of the probe beam and $C=B\exp(-i2\pi Z_2/\lambda_P)i\pi\omega_{1P}^2/\lambda_P Z_2$. Substituting Eqs. (15)–(18) into Eq. (20) and carrying out numerical integration over g, the intensity $I(t)$ at the detector plane can be calculated as $I(t)=|U(Z_1+Z_2,t)|^2$.

The effect of the TL on the probe beam is only to induce a phase shift. The geometrical configuration of the probe and excitation beams defines the sensitivity of the TL method by means of m. This parameter can be modified either by changing ω_{1p} or ω. When $r=\omega_{1p}$, within which more than 86% of the probe beam power is included, the time dependence of the phase shift, assuming $g=1$, is $\Phi(1,t)$. The time-dependent phase shift is calculated using Eq. (15) or Eq. (17) for the sample and Eq. (16) or Eq. (18) for the air. The phase shifts calculated using the parameters of Table I with $g=1$ are shown in Fig. 7. Here the time scale is in units of t_c. One can see from Fig. 7 that the zero-order approximation for the phase shift created in the sample agrees with the first-order one. The relative difference is less than 0.3%. The air phase shift it is approximately 1.7% of that of the glass sample.

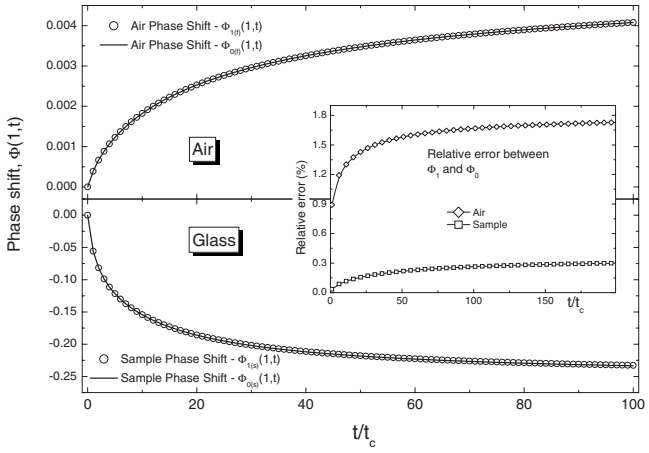

FIG. 7. Probe beam phase shift in air and in the sample calculated using order 0 and 1 approximations as a function of time. The inset shows the relative error between both approximations.

The relative difference between phase shifts calculated with zero- and first-order approximations is more important when the sample thickness is reduced. Figure 8 shows this difference at $t=0.12$ s as a function of the sample thickness. With a thin sample, boundary effects become important and the first order approximation should be used.

Finally, Fig. 9 shows the TL signal calculated using the analytical expressions and the phase shift. The agreement between the zero and first order approximations is again good when both the TL contributions from the air and the sample elements are taken into account. For the case where no air effect is included, the intensity transient deviates a little from the expected using the air coupling solution. This difference could lead to an overestimation of the thermal diffusivity and the parameter θ of approximately 2%.

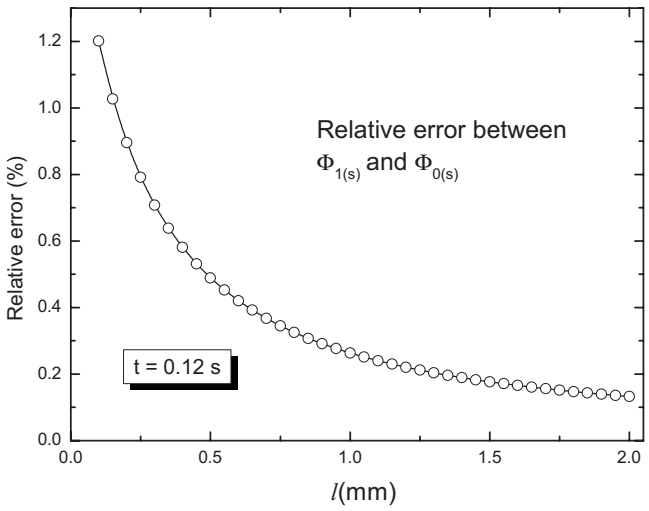

FIG. 8. Relative difference between the zero and first order approximations for the sample phase shift at $t=0.12$ s as a function of the sample thickness.

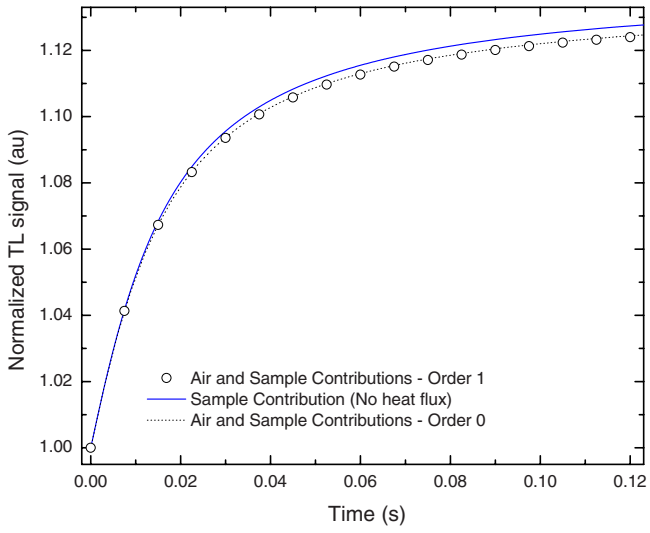

FIG. 9. (Color online) Normalized TL signal calculated using the approximations presented in Sec. III and the parameters listed in Table I. The sample thickness was $l=1$ mm.

IV. CONCLUSION

We presented analytical solutions for the temperature gradient induced by the TL effect considering both the heat transfer from sample to air and the TL generated in the air surroundings. Our analytical solution was found to agree with that of our FEA software. The results showed that heat transfer between the sample surface and the air coupling fluid does not introduce an important effect in the optical phase shift when compared with the solution obtained without considering the air-sample heat flux. On the other hand, when the TL created in the air coupling fluid is taken into account, a significant effect is introduced on the predicted time-dependent TL signals, which corresponds to approximately 1.7% of the sample's TL effect. The effect is due to finite heat transfer at the interface typically neglected in semi-infinite cylinder approximations. These solutions open up the possibility of applying the TL method for accurate prediction of the heat transfer to the coupling fluid and subsequently to study the gas surrounding the samples by using a known material solid sample.

[1]J. P. Gordon, R. C. C. Leite, R. S. Moore, S. P. S. Porto, and J. R. Whinnery, J. Appl. Phys. **36**, 3 (1965).
[2]R. D. Snook and R. D. Lowe, Analyst (Cambridge, U.K.) **120**, 2051 (1995).
[3]J. Shen, R. D. Lowe, and R. D. Snook, Chem. Phys. **165**, 385 (1992).
[4]S. E. Bialkowski, *Photothermal Spectroscopy Methods for Chemical Analysis* (Wiley, New York, 1996).
[5]*Progress in Photoacoustic and Photothermal Science and Technology*, edited by A. Mandelis (Elsevier, New York, 1991).
[6]D. P. Almond and P. M. Patel, *Photothermal Science and Techniques* (Chapman & Hall, London, 1996).
[7]M. L. Baesso, J. Shen, and R. D. Snook, J. Appl. Phys. **75**, 3732 (1994).
[8]M. Franko and C. D. Tran, Rev. Sci. Instrum. **67**, 1 (1996).
[9]J. Shen, M. L. Baesso, and R. D. Snook, J. Appl. Phys. **75**, 3738 (1994).
[10]M. L. Baesso, A. C. Bento, A. A. Andrade, J. A. Sampaio, E. Pecoraro, L. A. O. Nunes, T. Catunda, and S. Gama, Phys. Rev. B **57**, 10545 (1998).
[11]S. M. Lima, T. Catunda, R. Lebullenger, A. C. Hernandes, M. L. Baesso, A. C. Bento, and L. C. M. Miranda, Phys. Rev. B **60**, 15173 (1999).
[12]E. Peliçon, J. H. Rohling, A. N. Medina, A. C. Bento, M. L. Baesso, D. F. de Souza, S. L. Oliveira, J. A. Sampaio, S. M. Lima, L. A. O. Nunes, and T. Catunda, J. Non-Cryst. Solids **304**, 244 (2002).
[13]N. G. C. Astrath, J. H. Rohling, A. N. Medina, A. C. Bento, M. L. Baesso, C. Jacinto, T. Catunda, S. M. Lima, F. G. Gandra, M. J. V. Bell, and V. Anjos, Phys. Rev. B **71**, 214202 (2005).
[14]M. P. Belancon, L. C. Malacarne, P. R. B. Pedreira, A. N. Medina, M. L. Baesso, A. M. Farias, M. J. Barbosa, N. G. C. Astrath, and J. Shen, "Thermal Mirror and Thermal Lens Techniques for Semitransparent Material Charcterization," J. Phys.: Conf. Ser. (accepted).
[15]N. G. C. Astrath, L. C. Malacarne, P. R. B. Pedreira, A. C. Bento, M. L. Baesso, and J. Shen, Appl. Phys. Lett. **91**, 191908 (2007).
[16]L. C. Malacarne, F. Sato, P. R. B. Pedreira, A. C. Bento, R. S. Mendes, M. L. Baesso, N. G. C. Astrath, and J. Shen, Appl. Phys. Lett. **92**, 131903 (2008).
[17]F. Sato, L. C. Malacarne, P. R. B. Pedreira, M. P. Belancon, R. S. Mendes, M. L. Baesso, N. G. C. Astrath, and J. Shen, J. Appl. Phys. **104**, 053520 (2008).
[18]N. G. C. Astrath, F. B. G. Astrath, J. Shen, J. Zhou, P. R. B. Pedreira, L. C. Malacarne, A. C. Bento, and M. L. Baesso, Opt. Lett. **33**, 1464 (2008).
[19]O. O. Dada and S. E. Bialkowski, Appl. Spectrosc. **62**, 1326 (2008).
[20]O. O. Dada, M. R. Jorgensen, and S. E. Bialkowski, Appl. Spectrosc. **61**, 1373 (2007).
[21]P. R. Joshi, O. O. Dada, and S. E. Bialkowski, Appl. Spectrosc. **63**, 815 (2009).
[22]D. R. Lide, *CRC Handbook of Chemistry and Physics*, 88th ed. (CRC, Cleveland, 1977).